# Supplemental - Multi-season evaluation of temperature and wind in the marine boundary layer along the United States northeast coast in the High-Resolution Rapid Refresh model

Bianca Adler[1,2], Laura Bianco[1,2], David D. Turner[3], Joseph Olson[3], Xia Sun[1,3], Joshua Gebauer[4,5], Nicola Bodini[6], Stefano Letizia[6], and James M. Wilczak[2]

[1]Cooperative Institute for Research in Environmental Sciences (CIRES), University of Colorado Boulder, Boulder, CO, USA
[2]NOAA Physical Sciences Laboratory, Boulder, CO, USA
[3]NOAA Global Systems Laboratory, Boulder, CO, USA
[4]Cooperative Institute for Severe and High-Impact Weather Research and Operations, University of Oklahoma, Norman, OK, USA
[5]NOAA National Severe Storms Laboratory, Norman, OK, USA
[6]National Laboratory of the Rockies (NLR), Golden, CO, USA

**Correspondence:** Bianca Adler (bianca.adler@colorado.edu)

## S1 Comparison of OSTIA SST with in situ buoy measurements

Daily values of OSTIA SST at the grid points closest to the location of two buoys was extracted. Buoyz01 was located in the southern part of the investigation area further offshore and Buoy44085 was located closer to the coast in the northern part of the area. Daily averages of the buoy water temperature measurements were computed and compared against the OSTIA SST (Fig. S1).

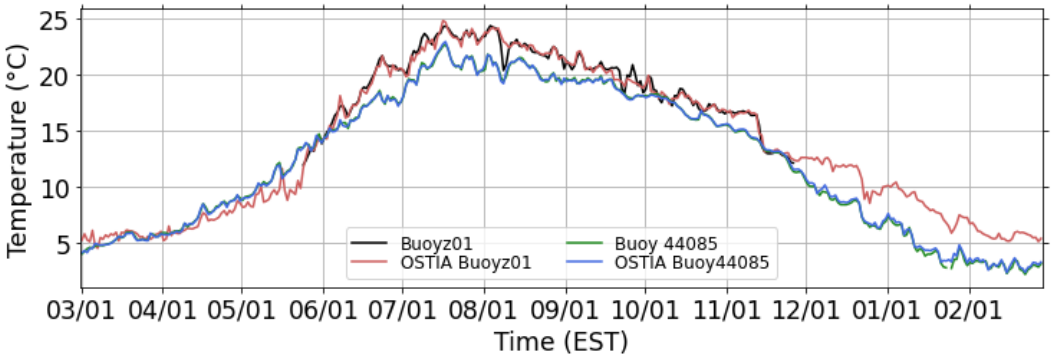


**Figure S1.** Time series of in situ water temperature measured at buoys and OSTIA sea surface temperature (SST) at grid points closest to the buoy locations during the investigation period. Data from Buoyz01 was only available between the end of May and the end of November 2024.

## S2 Comparison of WINDoe retrievals with individual input data

We use WINDoe to combine wind speed profile information from four different data sets, namely high- and low-resolution radar wind profiler data and scanning and profiling lidar. Each of these data sets has different specifics in terms of scan volume, vertical range, and temporal resolution. In addition the lidars and radar wind profilers are sensitive to completely different scatterers. It thus cannot be expected that they all provide exactly the same wind speed profiles. We compare the wind speed retrieved with WINDoe with the wind speed data from the individual inputs, which are available on Wind Data Hub. Table 1 overviews the data sets used for creating the WINDoe retrievals.

**Table 1.** Data sets combined in the WINDoe retrieval. For each site the instrument type, naming convention on the Wind Data Hub and DOI are given. Data sets can be accessed online by using the naming convention as in this example: https://wdh.energy.gov/ds/wfip3/rhod.sonic.z01.c0.

| Site | Radar wind profiler | Scanning Doppler lidar | Profiling Doppler lidar | Surface tower |
|---|---|---|---|---|
| NANT | nant.rwp.z01.c1<br>10.21947/2569390 | nant.lidar.z01.00<br>10.21947/2228417 | nant.lidar.z03.b0<br>10.21947/2447059 | nant.rad.z01.a0<br>10.21947/2323882 |
| BLOC | bloc.rwp.z01.c1<br>10.21947/2569230 | bloc.lidar.z01.a0<br>10.21947/2229436 | bloc.lidar.z03.c0<br>10.21947/2229426 | bloc.met.z01.c1<br>10.21947/2569867 |
| RHOD | rhod.rwp.z01.00<br>10.21947/2229548 | rhod.lidar.z01.a0<br>10.21947/2228755 | rhod.lidar.z03.00<br>10.21947/2228964 | rhod.sonic.z01.c0<br>10.21947/2307824 |

Figure S2 shows the relationship between the WINDoe wind speed on the y-axis and the wind speed from the individual inputs on the x-axis at all 3 sites in the lowest 1500 m. Data were linearly interpolated on the same height grid with 10 m grid spacing and to the same hourly time stamps. The correlation is very high, with Pearson correlation coefficients regularly exceeding 0.95, and neither the radar wind profiler nor scanning lidar data sets show a systematic bias. Only at the low heights where the profiling lidar provides information, retrieved wind speed are slightly lower (by about -0.2 $\mathrm{m\,s^{-1}}$) than the input data. Mean absolute errors (MAE) are mostly well below 1 $\mathrm{ms^{-1}}$, with the exception of the RHOD where MAE are close to 1 $\mathrm{m\,s^{-1}}$. This means that the differences between the retrieved wind speed and the individual input data is within the uncertainty of the retrieved profiles where the 1-$\sigma$ uncertainty is between 0.8 and 1.5 $\mathrm{m\,s^{-1}}$ in the lowest 1500 m on the average.

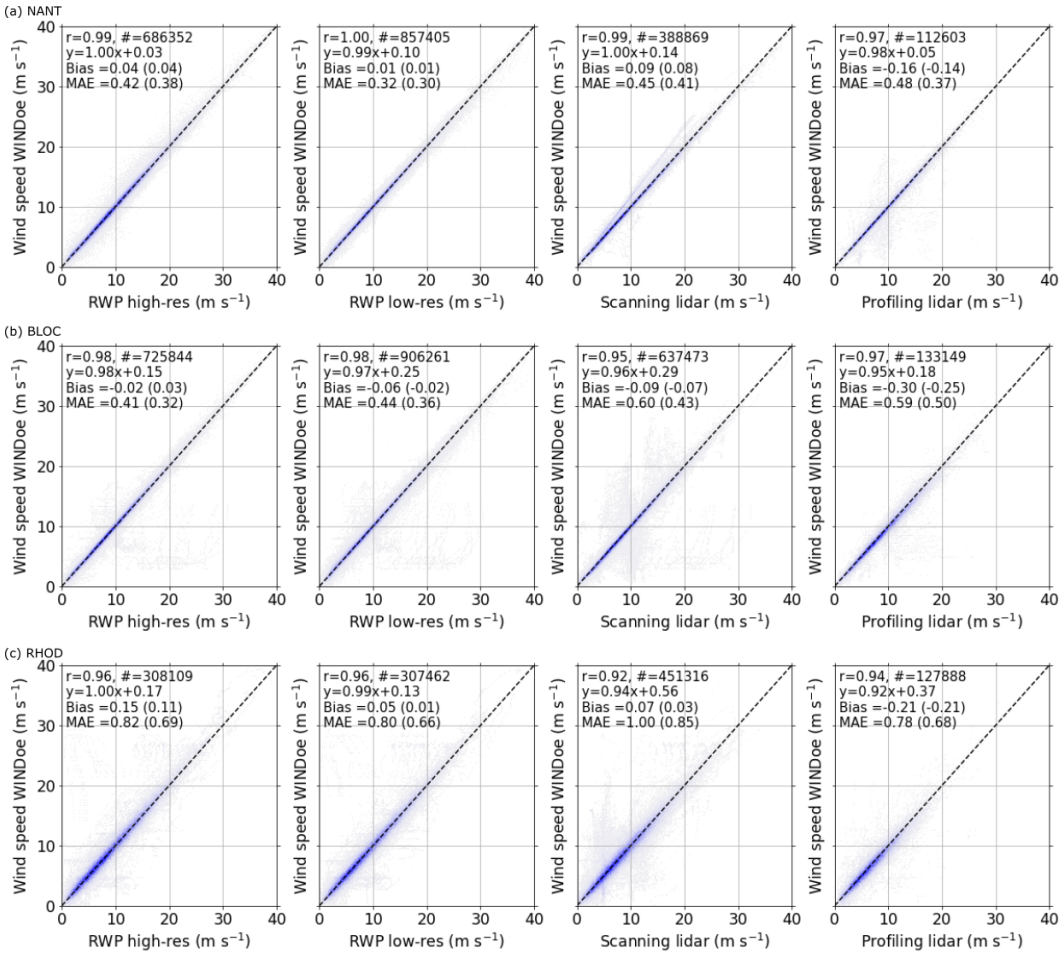


**Figure S2.** Relationship between wind speed from the WINDoe retrieval and wind speed from the individual input sources which are radar wind profiler high-resolution mode (RWP high-res), radar wind profiler low-resolution model (RWP low-res), scanning lidar, and profiling lidar. Data are interpolated to a 10-m vertical height grid and 60 min temporal resolution. Only data below 1500 m are shown.

## S3 Composites of wind and temperature profiles at BLOC and RHOD

Monthly composite of the observed and simulated diurnal cycle of wind and temperature at BLOC and RHOD are computed using forecast hour 12 of the HRRR model. In addition, monthly composites of the difference in wind and temperature (model minus observations) are computed.

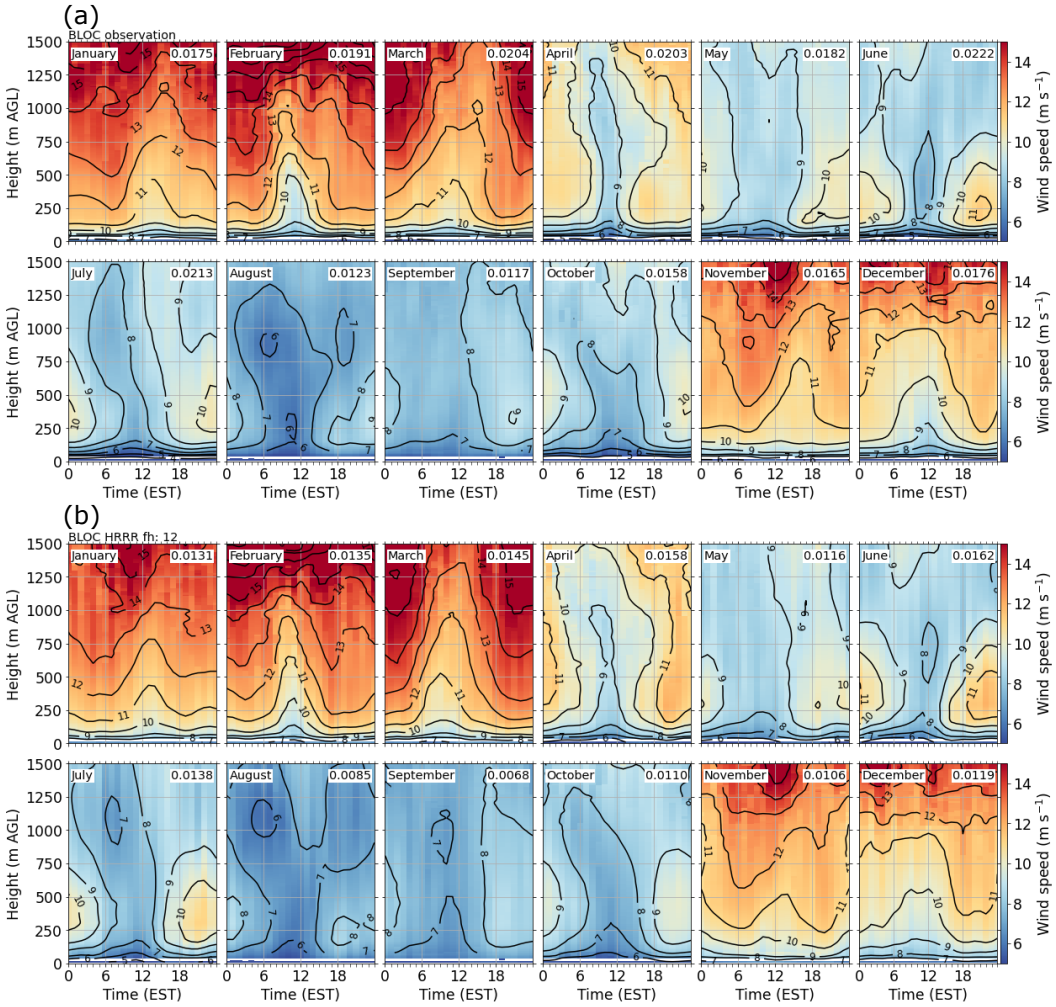


**Figure S3.** Monthly mean composites of (a) observed and (b) simulated horizontal wind speed (shading and contours) across the full diurnal range at BLOC. In (b), forecast hour 12 of the HRRR model is shown. Only times and heights where both model data and observations were available were used for computing the composites, and availability had to be at least 25 % for a time/height pair to be plotted. The number in the upper right corner of each subplot indicates the monthly mean shear in $\mathrm{s}^{-1}$ in the layer 50 to 200 m.

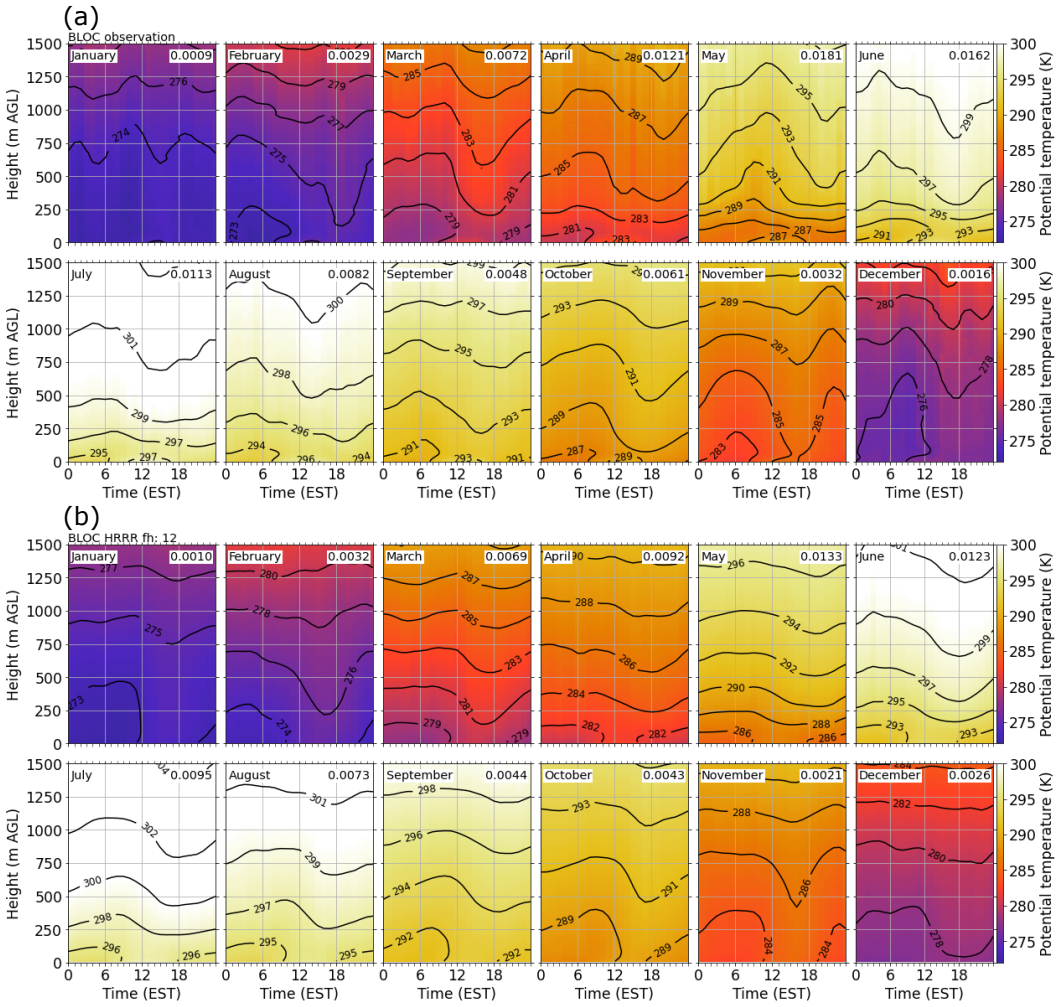


**Figure S4.** Monthly composites of (a) observed and (b) simulated potential temperature (shading and contours) across the full diurnal range at BLOC. In (b), forecast hour 12 of the HRRR model is shown. Only times and heights where both model data and observations were available were used for computing the composites, and availability had to be at least 25 % for a time/height pair to be plotted. The number in the upper right corner of each subplot indicates the monthly mean static stability in K $\mathrm{m}^{-1}$ in the layer between 100 m and 300 m.

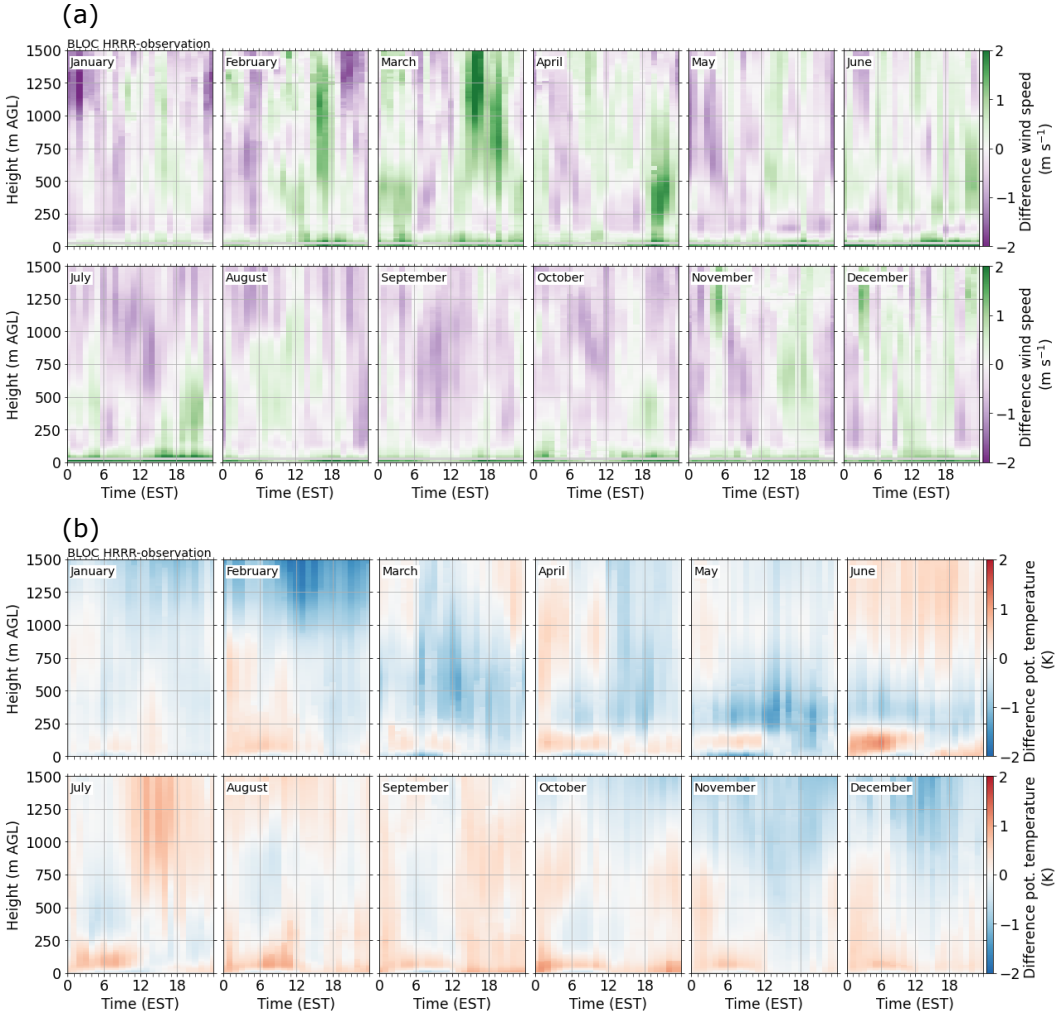


**Figure S5.** Monthly composites of HRRR model errors (model minus observation) of (a) horizontal wind speed and (b) potential temperature across the full diurnal range at BLOC. Forecast hour 12 of the HRRR model is shown. Availability had to be at least 25 % for a time/height pair to be plotted.

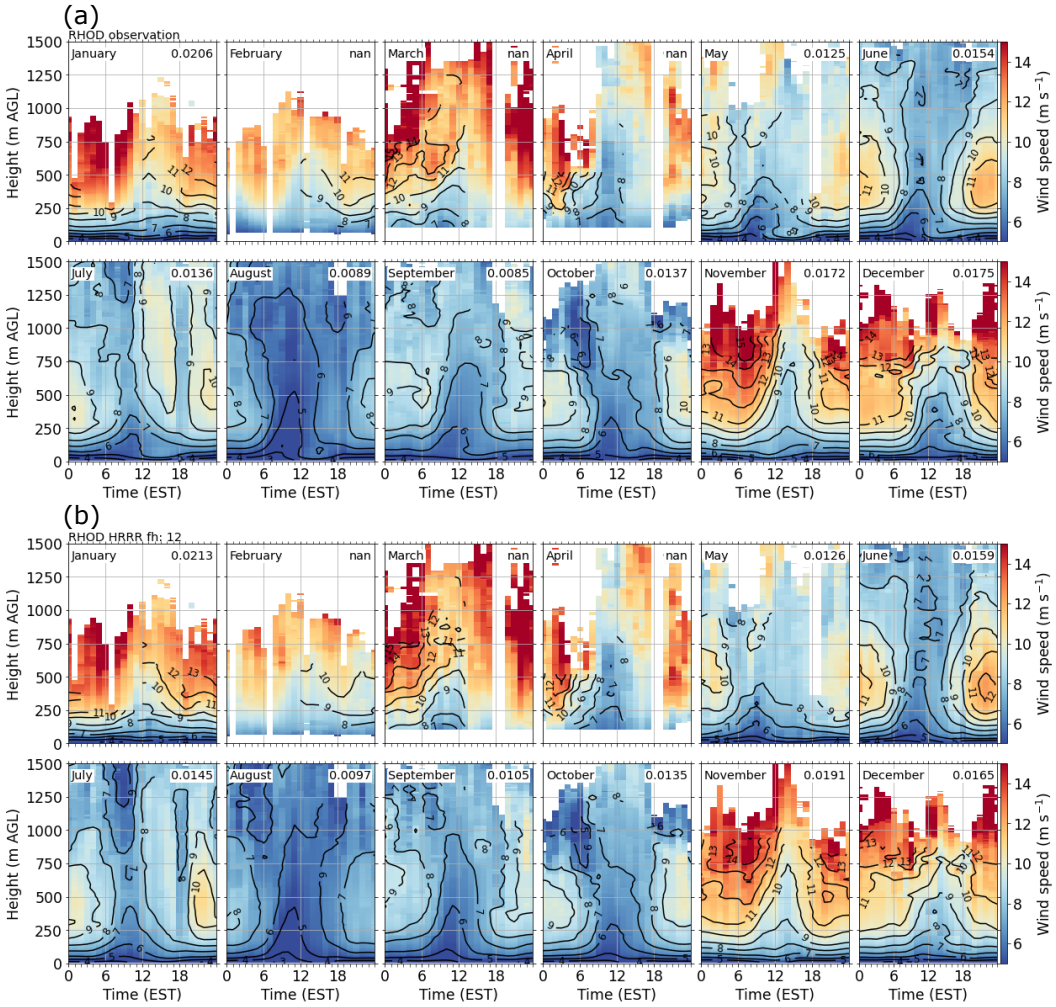


**Figure S6.** Monthly mean composites of (a) observed and (b) simulated horizontal wind speed (shading and contours) across the full diurnal range at RHOD. In (b), forecast hour 12 of the HRRR model is shown. Only times and heights where both model data and observations were available were used for computing the composites, and availability had to be at least 25 % for a time/height pair to be plotted. The number in the upper right corner of each subplot indicates the monthly mean shear in $\mathrm{s}^{-1}$ in the layer 50 to 200 m.

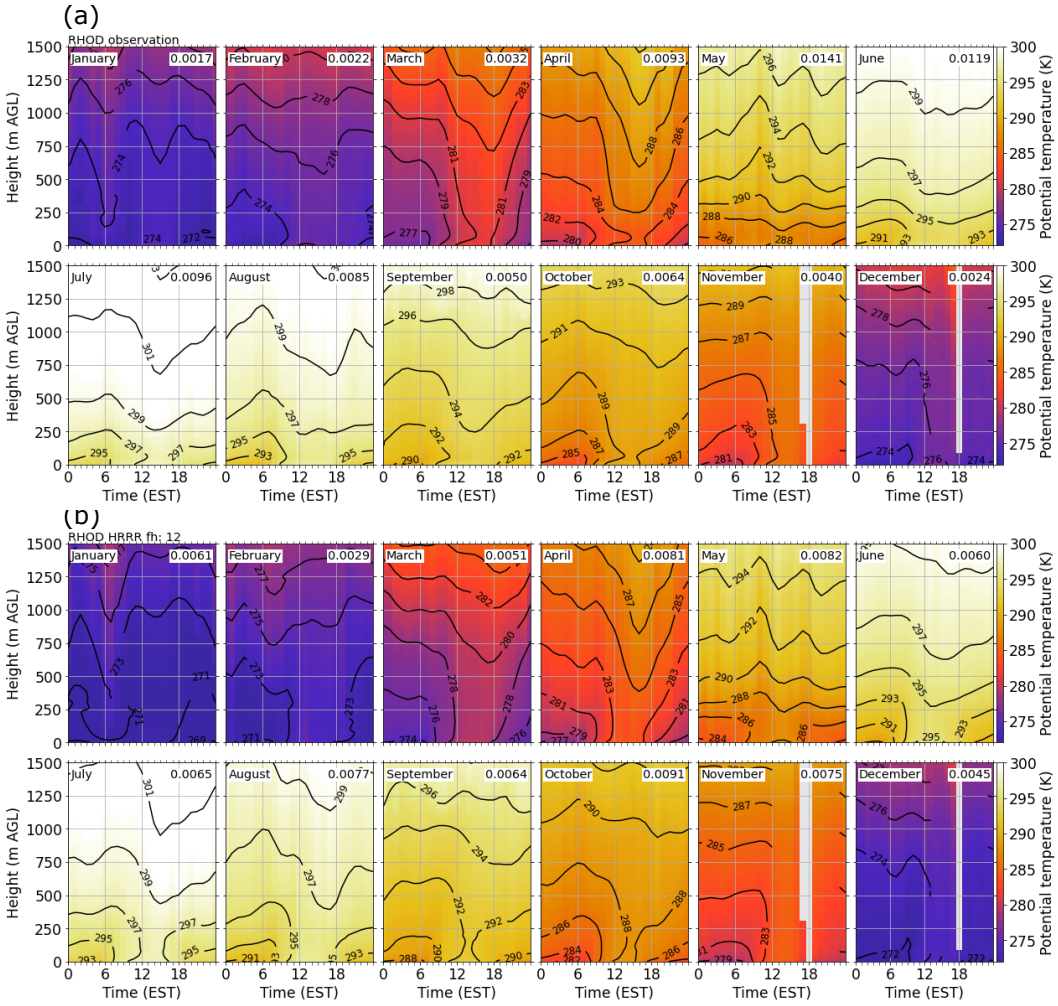


**Figure S7.** Monthly composites of (a) observed and (b) simulated potential temperature (shading and contours) across the full diurnal range at RHOD. In (b), forecast hour 12 of the HRRR model is shown. Only times and heights where both model data and observations were available were used for computing the composites, and availability had to be at least 25 % for a time/height pair to be plotted. The number in the upper right corner of each subplot indicates the monthly mean static stability in K $\mathrm{m}^{-1}$ in the layer between 100 m and 300 m.

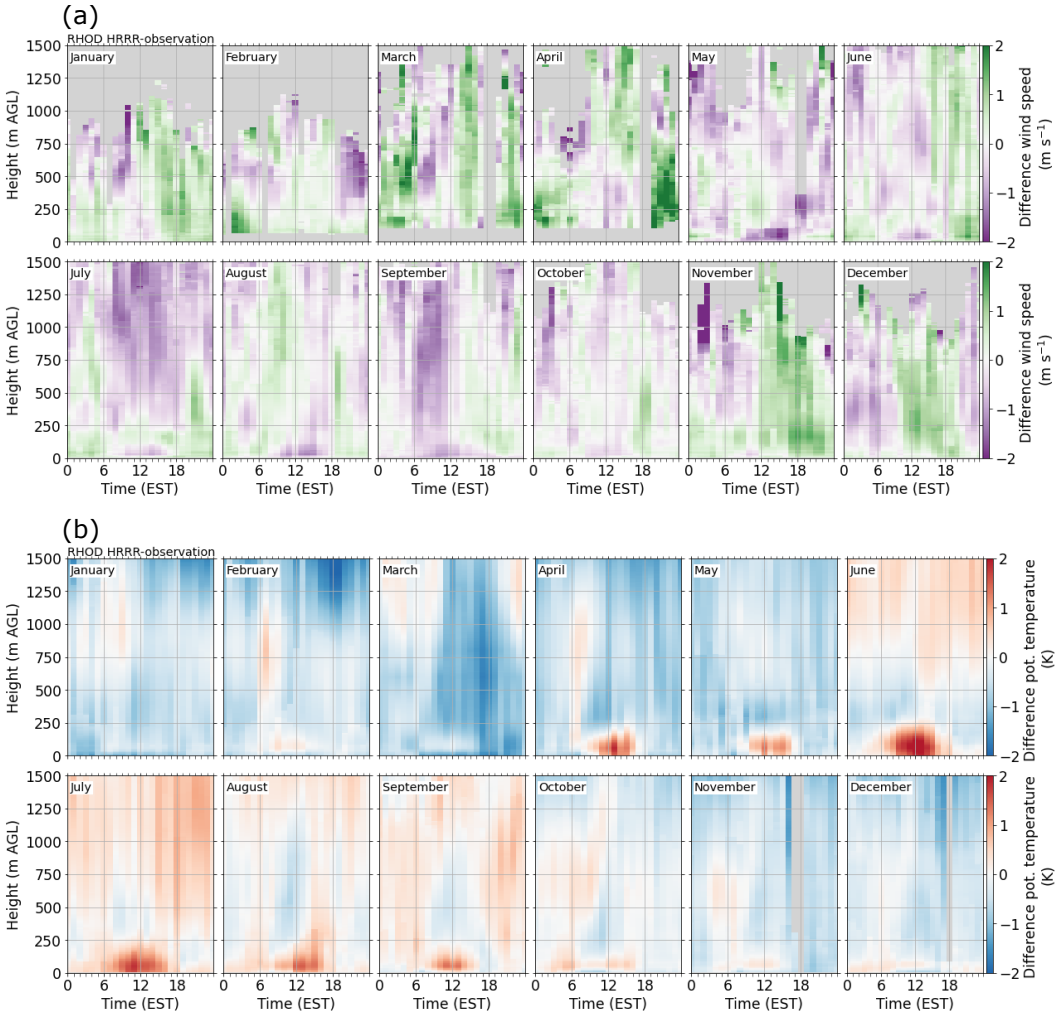


**Figure S8.** Monthly composites of HRRR model errors (model minus observation) of (a) horizontal wind speed and (b) potential temperature across the full diurnal range at RHOD. Forecast hour 12 of the HRRR model is shown. Availability had to be at least 25 % for a time/height pair to be plotted.

## S4 Low-level wind speed and temperature errors in dependence of wind direction

The relationship between HRRR model errors in wind speed shear and static stability and wind direction on the y-axis is computed for BLOC (Fig. S9) and RHOD (Fig. S10).

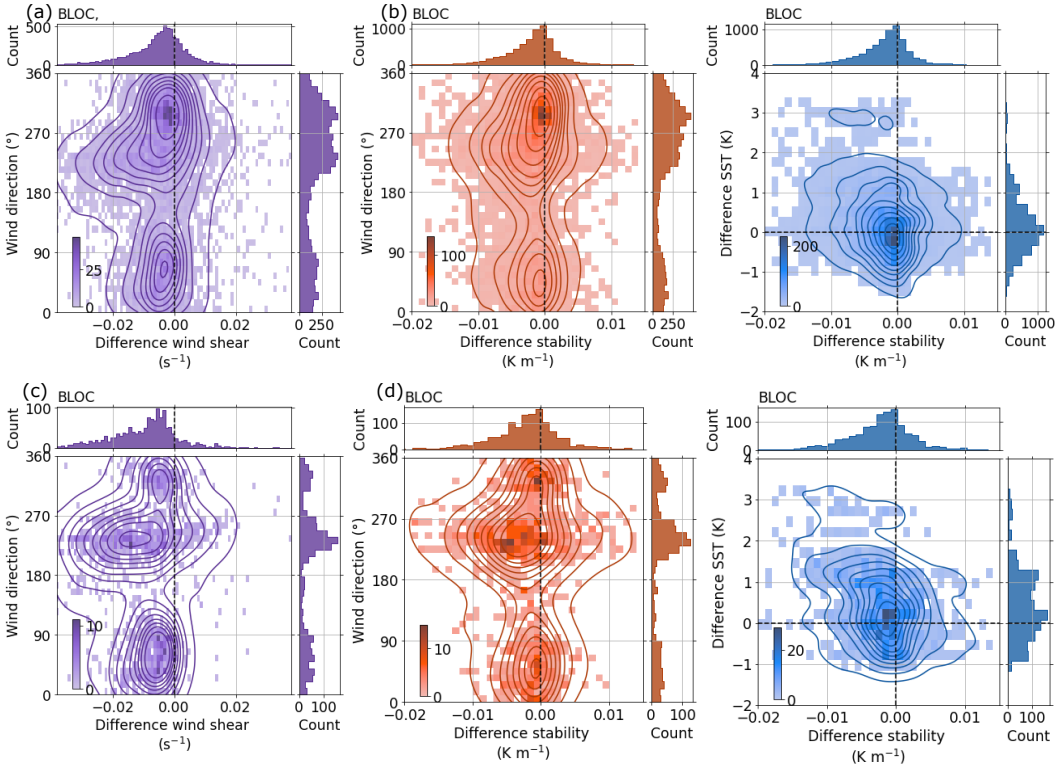


**Figure S9.** Relationship between the error (HRRR model minus observation) in (a,d) horizontal wind speed shear between the 50 m to 200 m layer and in (b,e) static stability computed as the virtual potential temperature gradient between 100 m and 300 m and observed wind direction averaged over the respective layer at BLOC. (c,f) Relationship between the error in stability in the 100 m to 300 m layer and the error in sea surface temperature (SST) (HRRR model minus OSTIA). The top row is for all available times, and the bottom row is when an LLJ is observed. Data at forecast hour 12 are shown for the HRRR model. Marginal axes show histograms.

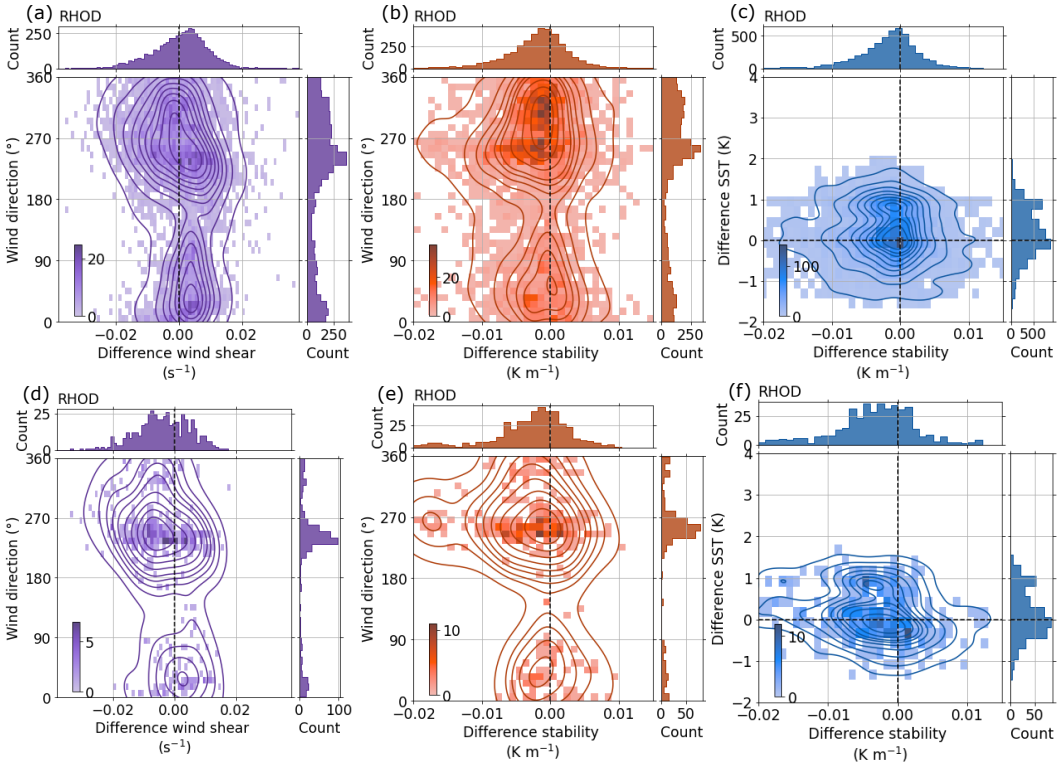


**Figure S10.** Relationship between the error (HRRR model minus observation) in (a,d) horizontal wind speed shear between the 50 m to 200 m layer and in (b,e) static stability computed as the virtual potential temperature gradient between 100 m and 300 m and observed wind direction averaged over the respective layer at RHOD. (c,f) Relationship between the error in stability in the 100 m to 300 m layer and the error in sea surface temperature (SST) (HRRR model minus OSTIA). The top row is for all available times, and the bottom row is when an LLJ is observed. Data at forecast hour 12 are shown for the HRRR model. Marginal axes show histograms.